

Theorem 2: If the incidence medium is lossless and the transmission medium is anelastic, then there are no critical angles.

If θ^I is a critical angle, then $\theta^T = \pi/2$. Because the incidence medium is elastic, by Snell's law, the attenuation vector in the transmission medium is perpendicular to the interface and, hence, to the direction of propagation. However, since the transmission medium is anelastic, such a wave cannot exist (see condition (3.36) and equation (3.118)).

The analysis about the existence of critical angles and the energy flow and dissipation of the different waves is given in detail in Chapter 6, where the reflection-transmission problem of SH waves in the symmetry planes of monoclinic media is discussed. The main results are that critical angles in anelastic media exist only under very particular conditions, and that interference fluxes are not present in the lossless case (see Section 6.1.7). Some researchers define the critical angle as the angle of incidence for which the propagation angle of the transmitted wave is $\pi/2$, i.e., when the wavenumber vector κ is parallel to the interface (e.g., Borcherdt, 1977; Wennerberg, 1985, Caviglia, Morro and Pagani, 1989). This is not correct from a physical point of view. In Chapter 6, we adopt the criterion that the Umov-Poynting vector or energy-flow direction is parallel to the interface, which is the criterion used in anisotropic media. The two definitions coincide only in particular cases, because, in general, the phase-velocity and energy-velocity directions do not coincide. Theorem 2 is still valid when using the second criterion since the attenuation and Umov-Poynting vectors can never be perpendicular in an anelastic medium (see equation (3.118)).

3.9 Memory variables and equation of motion

The memory-variable approach introduced in Section 2.7 is essential to avoid numerical calculations of time convolutions when modeling wave propagation in the time domain. With this approach, we obtain a complete differential formulation. The relaxation functions in the stress-strain relation (3.142) for isotropic media have the form (2.198). We set

$$\psi_K(t) = \mathcal{K}_\infty \left[1 - \frac{1}{L_1} \sum_{l=1}^{L_1} \left(1 - \frac{\tau_{el}^{(1)}}{\tau_{\sigma l}^{(1)}} \right) \exp(-t/\tau_{\sigma l}^{(1)}) \right] H(t), \quad (3.185)$$

$$\psi_\mu(t) = \mu_\infty \left[1 - \frac{1}{L_2} \sum_{l=1}^{L_2} \left(1 - \frac{\tau_{el}^{(2)}}{\tau_{\sigma l}^{(2)}} \right) \exp(-t/\tau_{\sigma l}^{(2)}) \right] H(t), \quad (3.186)$$

where $\tau_{el}^{(\nu)}$ and $\tau_{\sigma l}^{(\nu)}$ are relaxation times corresponding to dilatational ($\nu = 1$) and shear ($\nu = 2$) attenuation mechanisms. They satisfy the condition (2.169), $\tau_{el}^{(\nu)} \geq \tau_{\sigma l}^{(\nu)}$, with the equal sign corresponding to the elastic case.

In terms of the Boltzmann operation (2.6), equation (3.142) reads

$$\sigma_{ij} = \psi_K \odot \epsilon_{kk} \delta_{ij} + 2\psi_\mu \odot d_{ij}, \quad (3.187)$$

or,

$$\sigma_{ij} = \mathcal{K}_U \left(\epsilon_{kk} + \sum_{l=1}^{L_1} e_l^{(1)} \right) \delta_{ij} + 2\mu_U \left(d_{ij} + \sum_{l=1}^{L_2} e_{ijl}^{(2)} \right), \quad (3.188)$$

3.9 Memory variables and equation of motion

where

$$\mathcal{K}_U = \frac{\mathcal{K}_\infty}{L_1} \sum_{l=1}^{L_1} \frac{\tau_{el}^{(1)}}{\tau_{\sigma l}^{(1)}}, \quad \mu_U = \frac{\mu_\infty}{L_2} \sum_{l=1}^{L_2} \frac{\tau_{el}^{(2)}}{\tau_{\sigma l}^{(2)}}, \quad (3.189)$$

and

$$e_l^{(1)} = \varphi_{1l} * \epsilon_{kk}, \quad l = 1, \dots, L_1 \quad (3.190)$$

and

$$e_{ijl}^{(2)} = \varphi_{2l} * d_{ij}, \quad l = 1, \dots, L_2 \quad (3.191)$$

are sets of memory variables for dilatation and shear mechanisms, with

$$\check{\varphi}_{\nu l} = \frac{1}{\tau_{\sigma l}^{(\nu)}} \left(\sum_{l=1}^{L_\nu} \frac{\tau_{el}^{(\nu)}}{\tau_{\sigma l}^{(\nu)}} \right)^{-1} \left(1 - \frac{\tau_{el}^{(\nu)}}{\tau_{\sigma l}^{(\nu)}} \right) \exp(-t/\tau_{\sigma l}^{(\nu)}). \quad (3.192)$$

As in the 1-D case (see equation (2.292)), the memory variables satisfy

$$e_l^{(1)} = \varphi_{1l}(0) \epsilon_{kk} - \frac{e_l^{(1)}}{\tau_{\sigma l}^{(1)}}, \quad e_{ijl}^{(2)} = \varphi_{2l}(0) d_{ij} - \frac{e_{ijl}^{(2)}}{\tau_{\sigma l}^{(2)}}. \quad (3.193)$$

For $n = 2$ and say, the (x, z) -plane, we have three independent sets of memory variables. In fact, since $d_{11} = -d_{33} = (\epsilon_{11} - \epsilon_{33})/2$, then $e_{11l}^{(2)} = \varphi_{2l} * d_{11} = -\varphi_{2l} * d_{33}$. The other two sets are $e_l^{(1)} = \varphi_{1l} * \epsilon_{kk}$ and $e_{13l}^{(2)} = \varphi_{2l} * \epsilon_{13}$. In 3-D space ($n = 3$), there are six sets of memory variables, since $d_{11} + d_{22} + d_{33} = 0$ implies $e_{11l}^{(2)} + e_{22l}^{(2)} + e_{33l}^{(2)} = 0$, and two of these sets are independent. The other four sets are $e_l^{(1)} = \varphi_{1l} * \epsilon_{kk}$, $e_{23l}^{(2)} = \varphi_{2l} * \epsilon_{23}$, $e_{13l}^{(2)} = \varphi_{2l} * \epsilon_{13}$ and $e_{12l}^{(2)} = \varphi_{2l} * \epsilon_{12}$.

The equation of motion in 3-D space is obtained by substituting the stress-strain relation (3.188) into Euler's differential equations (1.23),

$$\begin{aligned} \partial_t^2 u_1 &= \rho^{-1} (\partial_1 \sigma_{11} + \partial_2 \sigma_{12} + \partial_3 \sigma_{13} + f_1) \\ \partial_t^2 u_2 &= \rho^{-1} (\partial_1 \sigma_{12} + \partial_2 \sigma_{22} + \partial_3 \sigma_{23} + f_2) \\ \partial_t^2 u_3 &= \rho^{-1} (\partial_1 \sigma_{13} + \partial_2 \sigma_{23} + \partial_3 \sigma_{33} + f_3), \end{aligned} \quad (3.194)$$

and making use of the strain-displacement relations (1.2)

$$\epsilon_{ij} = \frac{1}{2} (\partial_i u_j + \partial_j u_i). \quad (3.195)$$

In 2-D space and in the (x, z) -plane, all the derivatives ∂_2 vanish, u_2 is constant, and we should consider the first and third equations in (3.194). Applications of this modeling algorithm to compute the seismic response of reservoir models can be found in Kang and McMechan (1993), where Q effects are shown to be significant in both surface and offset vertical seismic profile data.

Assuming $L_1 = L_2$ and grouping the memory variables in the equation for each displacement component, the number of memory variables can be reduced to 2 in 2-D space and 3 in 3-D space (Xu and McMechan, 1995). Additional memory-storage savings can be achieved by setting $\tau_{\sigma l}^{(1)} = \tau_{\sigma l}^{(2)}$ (Emmerich and Korn, 1987). To further reduce storage, only a single relaxation time can be assigned to each grid point if a direct method is used to solve the viscoacoustic equation of motion (Day, 1998). A suitable spatial distribution of these relaxation times simulates the effects of the full relaxation spectrum.

3.6 The correspondence principle

The correspondence principle allows us to obtain viscoelastic solutions from the corresponding elastic (lossless) solutions. The stress-strain relation (3.2) can be rewritten as

$$\sigma_{ij} = \psi_K * \partial_t \epsilon_{kk} \delta_{ij} + 2\psi_\mu * \partial_t d_{ij}, \quad (3.142)$$

where d_{ij} is defined in equation (3.6).

Note that the Fourier transform of the stress-strain relations (3.142) is

$$\sigma_{ij}(\omega) = \mathcal{K}(\omega) \epsilon_{kk}(\omega) \delta_{ij} + 2\mu(\omega) d_{ij}(\omega), \quad (3.143)$$

where

$$\mathcal{K}(\omega) = \mathcal{F}[\partial_t \psi_K(t)] \quad \text{and} \quad \mu(\omega) = \mathcal{F}[\partial_t \psi_\mu(t)] \quad (3.144)$$

are the corresponding complex moduli. The form (3.143) is similar to the stress-strain relation of linear elasticity theory, except that the moduli are complex and frequency dependent. Note also that Euler's differential equations (1.23) are the same for lossy and lossless media. Therefore, if the elastic solution is available, the viscoelastic solution is obtained by replacing the elastic moduli with the corresponding viscoelastic moduli. This is known as the correspondence principle². We show specific examples of this principle in Section 3.10. Extensions of the correspondence principle are given in Golden and Graham (1988, p. 68).

3.7 Rayleigh waves

The importance of Rayleigh waves can be noted in several fields, from earthquake seismology to material science (Parker and Maugin, 1988; Chadwick, 1989). The first theoretical investigations carried out by Lord Rayleigh (1885) in isotropic elastic media showed that these waves are confined to the surface and, therefore, they do not scatter in depth as do seismic body waves.

Hardtwig (1943) was the first to study viscoelastic Rayleigh waves, though he erroneously restricts their existence to a particular choice of the complex Lamé parameters. Scholte (1947) rectifies this mistake and verifies that the waves always exist in viscoelastic solids. He also predicts the existence of a second surface wave, mainly periodic with depth, whose exponential damping is due to anelasticity and not to the Rayleigh character – referred to later as v.e. mode. Caloi (1948) and Horton (1953) analyze the anelastic characteristics and displacements of the waves considering a Voigt-type dissipation mechanism with small viscous damping, and a Poisson solid. Borcherdt (1973) analyzes the particle motion at the free surface and concludes that the differences between elastic and viscoelastic Rayleigh waves arise from differences in their components: the usual inhomogeneous plane waves in the elastic case, and viscoelastic inhomogeneous plane waves in the anelastic case, which allow any angle between the propagation and attenuation vectors.

²Although the principle has been illustrated for isotropic media, its extension to the anisotropic case can be obtained by taking the Fourier transform of the stress-strain relation (2.22), which leads to equation (4.4).

3.7 Rayleigh waves

A complete analysis is carried out by Currie, Hayes and O'Leary (1977), Currie and O'Leary (1978) and Currie (1979). They show that for viscoelastic Rayleigh waves: (i) more than one wave is possible, (ii) the particle motion may be either direct or retrograde at the surface, (iii) the motion may change sense at many or no levels with depth, (iv) the wave energy velocity may be greater than the body waves energy velocities. They refer to the wave that corresponds to the usual elastic surface wave as quasi-elastic (q.e.), and to the wave that only exists in the viscoelastic medium as viscoelastic (v.e.). This mode is possible only for certain combinations of the complex Lamé constants and for a given range of frequencies. Using the method of generalized rays, Borejko and Ziegler (1988) study the characteristics of the v.e. surface waves for the Maxwell and Kelvin-Voigt solids.

3.7.1 Dispersion relation

Since the medium is isotropic, we assume without loss of generality that the wave propagation is in the (x, z) -plane with $z = 0$ being the free surface. Let a plane-wave solution to equation (1.23) be of the form

$$\mathbf{u} = \mathbf{U} \exp[i(\omega t - \mathbf{k} \cdot \mathbf{x})]. \quad (3.145)$$

For convenience, let $m = 1$ denote the compressional wave and $m = 2$ the shear wave. We rewrite the dispersion relations (3.24) as

$$k^{(m)2} = \frac{\omega^2}{v_m^2}, \quad v_1^2 = \frac{\mathcal{E}}{\rho}, \quad v_2^2 = \frac{\mu}{\rho}, \quad (3.146)$$

where $\mathcal{E}(\omega) = \lambda(\omega) + 2\mu(\omega)$.

A general solution is given by the superposition of the compressional and shear modes,

$$\mathbf{u} = \mathbf{U}^{(m)} \exp[i(\omega t - \mathbf{k}^{(m)} \cdot \mathbf{x})], \quad (3.147)$$

where

$$\mathbf{U}^{(1)} = U_0 \mathbf{k}^{(1)}, \quad \mathbf{U}^{(2)} \cdot \mathbf{k}^{(2)} = 0. \quad (3.148)$$

At the free surface ($z = 0$), the boundary conditions are

$$\sigma_{33} = \lambda \partial_1 u_1 + (\lambda + 2\mu) \partial_3 u_3 = 0, \quad \text{and} \quad \sigma_{13} = \mu(\partial_1 u_3 + \partial_3 u_1) = 0. \quad (3.149)$$

These boundary conditions imply that the horizontal wavenumber is the same for each mode,

$$k_1^{(1)} = k_1^{(2)} \equiv k_1 = \kappa_1 - i\alpha_1. \quad (3.150)$$

From equations (3.147) and (3.150), the displacement components are

$$\begin{aligned} u_1 &= F(z) \exp[i(\omega t - k_1 x)], & F(z) &= U_1^{(m)} \exp(-ik_3^{(m)} z), \\ u_3 &= G(z) \exp[i(\omega t - k_1 x)], & G(z) &= U_3^{(m)} \exp(-ik_3^{(m)} z), \end{aligned} \quad (3.151)$$

where the vertical wavenumbers are

$$k_3^{(m)} = \kappa_3^{(m)} - i\alpha_3^{(m)}. \quad (3.152)$$

2.4 Mechanical models and wave propagation

A typical creep function versus time, as well as a dissipation factor versus frequency are shown in Figure 2.1. These behaviors can be described by using viscoelastic constitutive equations based on mechanical models. To construct a mechanical model, two types of basic elements are required: weightless springs – no inertial effects are present – that represent the elastic solid, and dashpots, consisting of loosely fitting pistons in cylinders filled with a viscous fluid. The simplest are the Maxwell and Kelvin-Voigt models. The Maxwell model was introduced by Maxwell (1867) when discussing the nature of viscosity in gases. Meyer (1874) and Voigt (1892) obtained the so-called Voigt stress-strain relation by generalizing the equations of classical elasticity. The mechanical model representation of the Voigt solid (the Kelvin-Voigt model) was introduced by Lord Kelvin (Kelvin, 1875).

The relaxation function can be obtained by measuring the stress after imposing a rapidly constant unit strain in a relaxed sample of the medium, i.e., $\epsilon = H(t)$, such that (2.28) becomes

$$\sigma(t) = \partial_t \psi(t) * H(t) = \psi(t) * \delta(t) = \psi(t). \quad (2.141)$$

A constant state of stress instantaneously applied to the sample ($\sigma = H(t)$), with the resulting strain being measured as a function of time, describes the creep experiment. The resulting time function is the creep function. That is

$$\epsilon(t) = \partial_t \chi(t) * H(t) = \chi(t) * \delta(t) = \chi(t). \quad (2.142)$$

There are materials for which creep continues indefinitely as time increases. If the limit $\partial_t \chi(t = \infty)$ is finite, permanent deformation occurs after the application of a stress field. Such behavior is akin to that of viscoelastic fluids. If that quantity is zero, the material is referred to as a viscoelastic solid. If χ increases indefinitely, the relaxation function ψ must tend to zero, according to (2.41). This is another criterion to distinguish between fluid and solid behavior: that is, for fluid-like materials ψ tends to zero; for solid-like materials, ψ tends to a finite value.

2.4.1 Maxwell model

The simplest series combination of mechanical models is the Maxwell model depicted in Figure 2.2. A given stress σ applied to the model produces a deformation ϵ_1 on the spring and a deformation ϵ_2 on the dashpot. The stress-strain relation in the spring is

$$\sigma = M_U \epsilon_1, \quad (2.143)$$

where M_U is the elasticity constant of the spring (M_e in equation (2.25)). The subindex U denotes “unrelaxed”. Its meaning will become clear in the following discussion. The stress-strain relation in the dashpot is

$$\sigma = \eta \partial_t \epsilon_2, \quad \eta \geq 0, \quad (2.144)$$

where η is the viscosity. Assuming that the total elongation of the system is $\epsilon = \epsilon_1 + \epsilon_2$, the stress-strain relation of the Maxwell element is

$$\frac{\partial_t \sigma}{M_U} + \frac{\sigma}{\eta} = \partial_t \epsilon. \quad (2.145)$$

2.4 Mechanical models and wave propagation

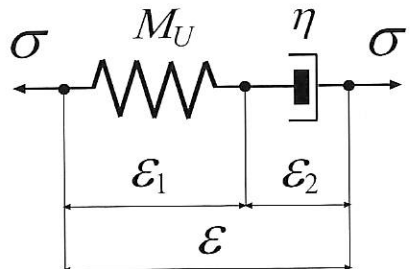


Figure 2.2: Mechanical model for a Maxwell material. The force on both elements is the same, but the elongation (strain) is different.

The Fourier transform of equation (2.145), or equivalently, the substitution of a harmonic wave $[\cdot] \exp(i\omega t)$, yields

$$\sigma = M\epsilon, \quad (2.146)$$

where

$$M(\omega) = \frac{\omega\eta}{\omega\tau - i} \quad (2.147)$$

is the complex modulus, with

$$\tau = \frac{\eta}{M_U} \quad (2.148)$$

being a relaxation time.

The corresponding relaxation function is

$$\psi(t) = M_U \exp(-t/\tau) H(t). \quad (2.149)$$

This can be verified by performing the Boltzmann operation (2.6),

$$\partial_t \psi = \psi \odot \delta = M_U \delta(t) - \frac{M_U}{\tau} \exp(-t/\tau) H(t), \quad (2.150)$$

and calculating the complex modulus (2.31),

$$\mathcal{F}[\partial_t \psi] = \int_{-\infty}^{\infty} \partial_t \psi \exp(-i\omega t) dt = M_U - \frac{M_U}{1 + i\omega\tau} = \frac{\omega\eta}{\omega\tau - i}. \quad (2.151)$$

The complex modulus (2.147) and the relaxation function (2.149) can be shown to satisfy all the requirements listed in Section 2.2.5. Using equations (2.41) and (2.42), we note that the creep function of the Maxwell model is

$$\chi(t) = \frac{1}{M_U} \left(1 + \frac{t}{\tau} \right) H(t). \quad (2.152)$$

The creep and relaxation functions are depicted in Figure 2.3a-b, respectively. As can be seen, the creep function is not representative of the real creep behavior in real solids. Rather, it resembles the creep function of a viscous fluid. In the relaxation

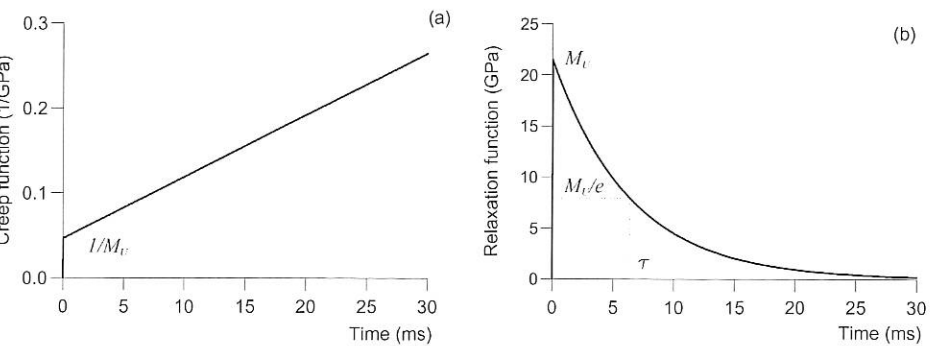


Figure 2.3: Creep (a) and relaxation (b) functions of the Maxwell model ($M_U = 2.16 \text{ GPa}$, $\tau = 1/(2\pi f)$, $f = 25 \text{ Hz}$). The creep function resembles the creep function of a viscous fluid. The system does not present an asymptotical residual stress as in the case of real solids.

experiment, both the spring and the dashpot experience the same force, and because it is not possible to have an instantaneous deformation in the dashpot, the extension is initially in the spring. The dashpot extends and the spring contracts, such that the total elongation remains constant. At the end, the force in the spring relaxes completely and the relaxation function does not present an asymptotical residual stress, as in the case of real solids. In conclusion, the Maxwell model appears more appropriate for representing a viscoelastic fluid. We can see from Figure 2.3a that M_U represents the instantaneous response of the system, hence, the name unrelaxed modulus.

We have seen in Section 2.3 that the partition of the second term in the right-hand side of equation (2.94) in terms of the rate of strain-energy density and rate of dissipated-energy density is, in general, not unique. We have claimed that the splitting (2.12) is consistent with the mechanical-model description of viscoelasticity. As an example, we verify the correctness of the general form (2.16) (or (2.96)) for the Maxwell model. Substituting the relaxation function (2.149) into that equation, we obtain

$$\begin{aligned} V(t) &= \frac{1}{2M_U} \left\{ \int_{-\infty}^t M_U \exp[-(t - \tau_1)/\tau] \partial_{\tau_1} \epsilon(\tau_1) d\tau_1 \right\}^2 = \\ &= \frac{1}{2M_U} \left\{ \int_{-\infty}^{\infty} \psi(t - \tau_1) \partial_{\tau_1} \epsilon(\tau_1) d\tau_1 \right\}^2 = \frac{1}{2M_U} (\psi * \partial_t \epsilon)^2 = \frac{\sigma^2}{2M_U}. \end{aligned} \quad (2.153)$$

But this is precisely the energy stored in the spring, since, using (2.143) and the form (2.93), we obtain

$$V = \frac{1}{2} M_U \epsilon_1^2 = \frac{\sigma^2}{2M_U}. \quad (2.154)$$

Note that because $\psi = \check{\psi} H$, the second term in the right-hand side of (2.94) can be written as

$$(\partial_t \psi * \epsilon) \partial_t \epsilon = \psi(0) \epsilon \partial_t \epsilon + (\partial_t \check{\psi} * \epsilon) \partial_t \epsilon. \quad (2.155)$$

2.4 Mechanical models and wave propagation

This is one possible partition and one may be tempted to identify the first term with the rate of strain-energy density. However, a simple calculation using the Maxwell model shows that this choice is not consistent with the energy stored in the spring.

The wave propagation properties are described by the phase velocity (2.83), the attenuation factor (2.85) and the quality factor (2.120). The quality factor has the simple expression

$$Q(\omega) = \omega \tau. \quad (2.156)$$

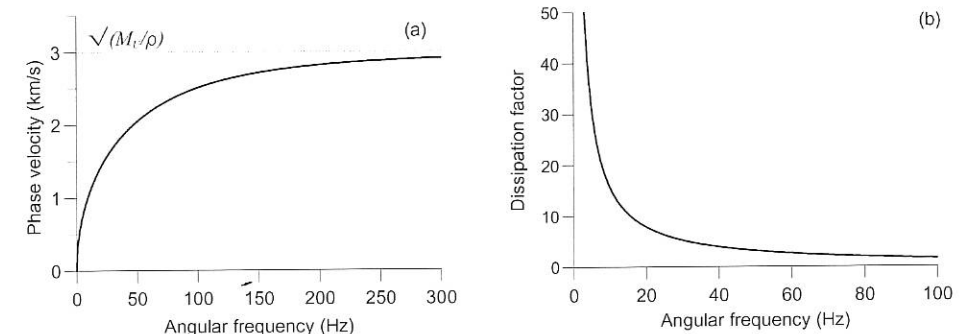


Figure 2.4: Phase velocity (a) and dissipation factor (b) of the Maxwell model ($M_U = \rho c^2$, $\rho = 2.4 \text{ gr/cm}^3$, $c = 3 \text{ km/s}$, $\tau = 1/(2\pi f)$, $f = 25 \text{ Hz}$). The system acts as a high-pass filter because low-frequency modes dissipate completely. The velocity for lossless media is obtained at the high-frequency limit. At low frequencies there is no propagation.

The phase velocity and dissipation factors are shown in Figures 2.4a-b, respectively. When $\omega \rightarrow 0$, then $v_p \rightarrow 0$, and $\omega \rightarrow \infty$ implies $v_p \rightarrow \sqrt{M_U/\rho}$, i.e., the velocity in the unrelaxed state. This means that a wave in a Maxwell material travels slower than a wave in the corresponding elastic material – if this is represented by the spring. The dissipation is infinite at zero frequency and the medium is lossless at high frequencies.

2.4.2 Kelvin-Voigt model

A viscoelastic model commonly used to describe anelastic effects is the Kelvin-Voigt stress-strain relation, which consists of a spring and a dashpot connected in parallel (Figure 2.5).

The total stress is composed of an elastic stress

$$\sigma_1 = M_R \epsilon, \quad (2.157)$$

where M_R is the spring constant – the subindex R denotes “relaxed” – and a viscous stress

$$\sigma_2 = \eta \partial_t \epsilon, \quad (2.158)$$

where ϵ is the total strain of the system. The stress-strain relation becomes

$$\sigma = \sigma_1 + \sigma_2 = M_R \epsilon + \eta \partial_t \epsilon. \quad (2.159)$$

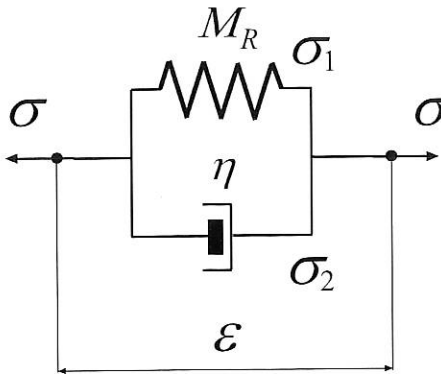


Figure 2.5: Mechanical model for a Kelvin-Voigt material. The strain on both elements is the same, but the forces are different.

The Fourier transform of (2.159) yields

$$\sigma = (M_R + i\omega\eta)\epsilon, \quad (2.160)$$

which identifies the complex modulus

$$M(\omega) = M_R + i\omega\eta. \quad (2.161)$$

The relaxation and creep functions are

$$\psi(t) = M_R H(t) + \eta\delta(t), \quad (2.162)$$

and

$$\chi(t) = \frac{1}{M_R} [1 - \exp(-t/\tau)] H(t), \quad (2.163)$$

where $\tau = \eta/M_R$.

The calculation of the relaxation function from (2.159) is straightforward, and the creep function can be obtained by using (2.41) and (2.42) and Fourier-transform methods. The two functions are represented in Figure 2.6a-b, respectively.

The relaxation function does not show any time dependence. This is the case of pure elastic solids. The delta function implies that, in practice, it is impossible to impose an instantaneous strain on the medium. In the creep experiment, initially the dashpot extends and begins to transfer the stress to the spring. At the end, the entire stress is on the spring. The creep function does not present an instantaneous strain because the dashpot cannot move instantaneously. This is not the case of real solids. The creep function tends to the relaxed modulus M_R at infinite time.

The quality factor (2.120) is

$$Q(\omega) = (\omega\tau)^{-1}. \quad (2.164)$$

Comparing this equation to equation (2.156) shows that the quality factors of the Kelvin-Voigt and Maxwell models are reciprocal functions.

2.4 Mechanical models and wave propagation

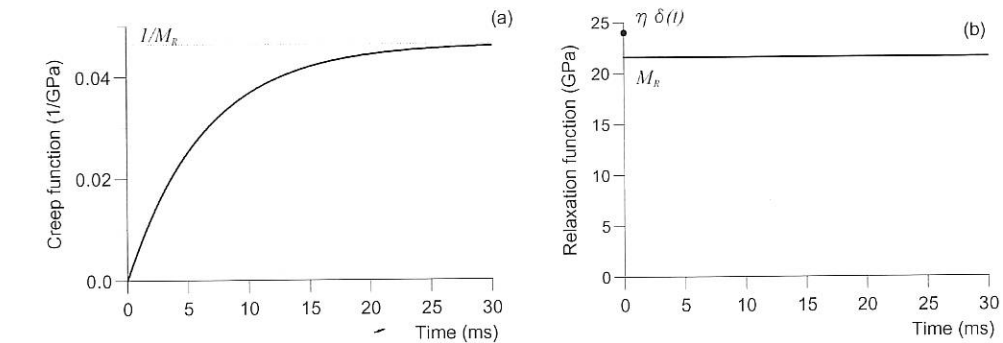


Figure 2.6: Creep (a) and relaxation (b) functions of the Kelvin-Voigt model ($M_R = 2.16$ GPa, $\tau = 1/(2\pi f)$, $f = 25$ Hz). The creep function lacks the instantaneous response of real solids. The relaxation function presents an almost elastic behavior.

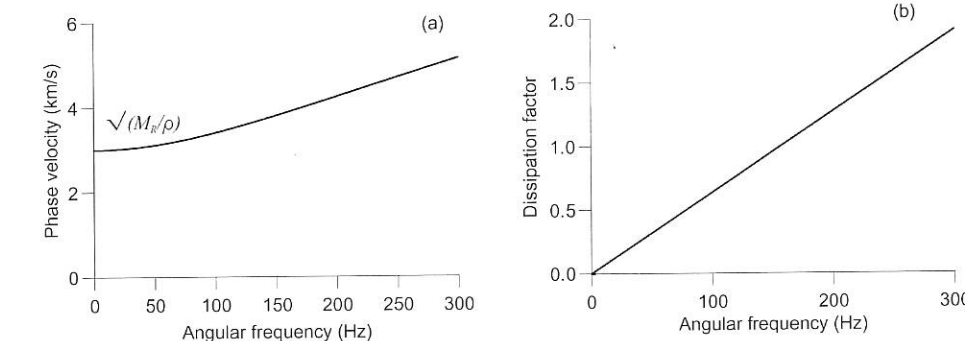


Figure 2.7: Phase velocity (a) and dissipation factor (b) of the Kelvin-Voigt model ($M_R = \rho c^2$, $\rho = 2.4$ gr/cm³, $c = 3$ km/s, $\tau = 1/(2\pi f)$, $f = 25$ Hz). The system acts as a low-pass filter because high-frequency modes dissipate completely. The elastic (lossless) velocity is obtained at the low-frequency limit. High frequencies propagate with infinite velocity.

The phase velocity and dissipation factor are displayed in Figure 2.7a-b.
The Kelvin-Voigt model can be used to approximate the left slope of a real relaxation peak (see Figure 2.1). The phase velocity $v_p \rightarrow \sqrt{M_R/\rho}$ for $\omega \rightarrow 0$, and $v_p \rightarrow \infty$ for $\omega \rightarrow \infty$, which implies that a wave in a Kelvin-Voigt material travels faster than a wave in the corresponding elastic material.

2.4.3 Zener or standard linear solid model

A series combination of a spring and a Kelvin-Voigt model gives a more realistic representation of material media, such as rocks, polymers and metals. The resulting system, called the Zener model (Zener, 1948) or standard linear solid, is shown in Figure 2.8. This model was introduced by Poynting and Thomson (1902).

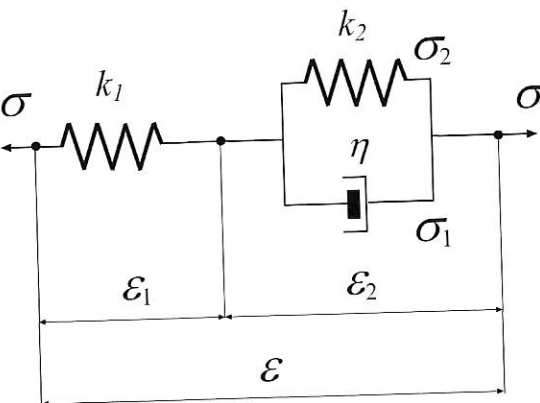


Figure 2.8: Mechanical model for a Zener material.

The stress-strain relations for the single elements are

$$\begin{aligned}\sigma &= k_1 \epsilon_1, \\ \sigma_1 &= \eta \partial_t \epsilon_2, \\ \sigma_2 &= k_2 \epsilon_2,\end{aligned}\quad (2.165)$$

with $k_1 \geq 0$, $k_2 \geq 0$ and $\eta \geq 0$. Moreover,

$$\sigma = \sigma_1 + \sigma_2, \quad \epsilon = \epsilon_1 + \epsilon_2. \quad (2.166)$$

The solution of these equations for σ and ϵ gives the stress-strain relation

$$\sigma + \tau_\sigma \partial_t \sigma = M_R(\epsilon + \tau_\epsilon \partial_t \epsilon), \quad (2.167)$$

where

$$M_R = \frac{k_1 k_2}{k_1 + k_2}, \quad (2.168)$$

is the relaxed modulus, and

$$\tau_\sigma = \frac{\eta}{k_1 + k_2}, \quad \tau_\epsilon = \frac{\eta}{k_2} \geq \tau_\sigma \quad (2.169)$$

2.4 Mechanical models and wave propagation

are the relaxation times.

As in the previous models, the complex modulus is obtained by performing a Fourier transform of the stress-strain relation (2.167),

$$M(\omega) = M_R \left(\frac{1 + i\omega\tau_\epsilon}{1 + i\omega\tau_\sigma} \right). \quad (2.170)$$

The relaxed modulus M_R is obtained for $\omega = 0$, and the unrelaxed modulus

$$M_U = M_R \left(\frac{\tau_\epsilon}{\tau_\sigma} \right), \quad (M_U \geq M_R) \quad (2.171)$$

for $\omega \rightarrow \infty$.

The stress-strain and strain-stress relations are

$$\sigma = \psi * \partial_t \epsilon, \quad \epsilon = \chi * \partial_t \sigma, \quad (2.172)$$

where the relaxation and creep functions are

$$\psi(t) = M_R \left[1 - \left(1 - \frac{\tau_\epsilon}{\tau_\sigma} \right) \exp(-t/\tau_\sigma) \right] H(t) \quad (2.173)$$

and

$$\chi(t) = \frac{1}{M_R} \left[1 - \left(1 - \frac{\tau_\sigma}{\tau_\epsilon} \right) \exp(-t/\tau_\epsilon) \right] H(t). \quad (2.174)$$

(As an exercise, the reader may obtain the complex modulus (2.170) by using equations (2.31) and (2.173)). Note that by the symmetry of the strain-stress relation (2.167), exchanging the roles of τ_σ and τ_ϵ and substituting M_R for M_R^{-1} in equation (2.173), the creep function (2.174) can be obtained.

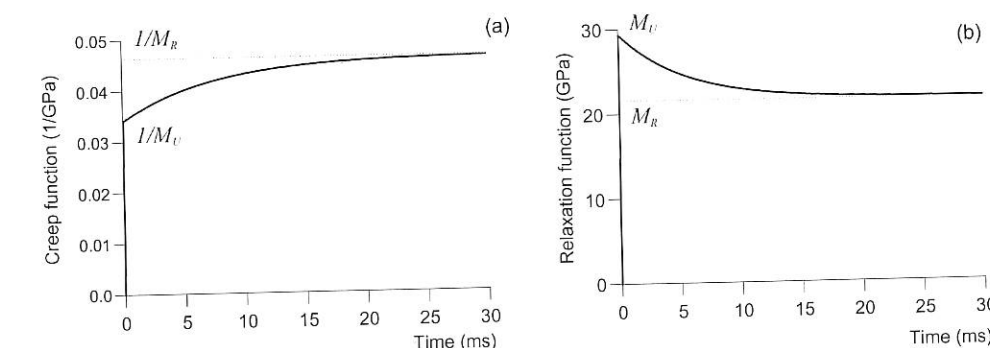


Figure 2.9: Creep (a) and relaxation (b) functions of the Zener model ($M_R = 2.16$ GPa, $M_U = 29.4$ GPa, $\tau_0 = 1/(2\pi f)$, $f = 25$ Hz). The creep function presents an instantaneous response and a finite asymptotic value as in real solids. The relaxation function presents an instantaneous unrelaxed state, and at the end of the process, the system has relaxed completely to the relaxed modulus M_R . The curve in (a) is similar to the experimental creep function shown in 2.1.

The relaxation and creep functions are represented in Figure 2.9a-b, respectively. In the creep experiment, there is an instantaneous initial value $\chi(0^+) = M_U^{-1}$, and an asymptotic strain $\chi(\infty) = M_R^{-1}$, determined solely by the spring constants. After the first initial displacement, the force across the dashpot is gradually relaxed by deformation therein, resulting in a gradual increase in the observed overall deformation; finally, the relaxation function exhibits an instantaneous asymptotic value is reached. Similarly, the relaxation function exhibits an instantaneous unrelaxed state of magnitude M_U . At the end of the process, the system has completely relaxed to the relaxed modulus M_R . Such a system, therefore, manifests the general features of the experimental creep function illustrated in Figure 2.1a. The relaxation function and complex modulus can be shown to satisfy all the requirements listed in Section 2.2.5.

The quality factor (2.120) is

$$Q(\omega) = \frac{1 + \omega^2 \tau_e \tau_\sigma}{\omega(\tau_e - \tau_\sigma)}, \quad (2.175)$$

where we have used equation (2.170).

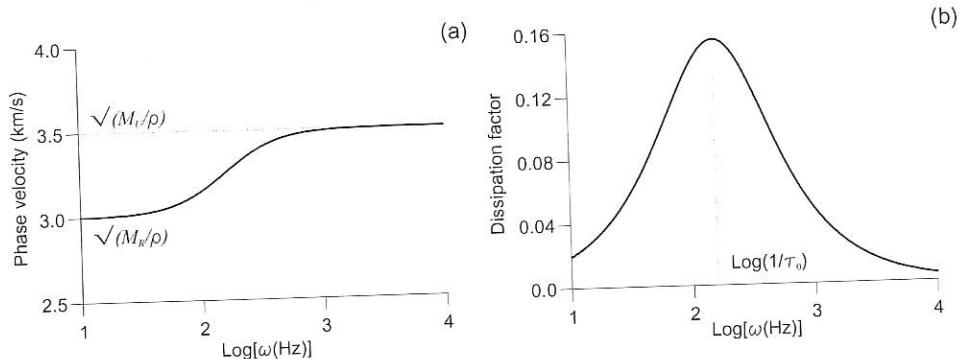


Figure 2.10: Phase velocity (a) and dissipation factor (b) of the Zener model. ($M_R = \rho c_R^2$, $\rho = 2.4$ g/cm³, $c_R = 3$ km/s, $M_U = \rho c_U^2$, $c_U = 3.5$ km/s, $\tau_0 = 1/(2\pi f)$, $f = 25$ Hz).

The phase velocity and dissipation factor Q^{-1} are shown in Figure 2.10a-b. The model has a relaxation peak at $\omega_0 = 1/\tau_0$, where

$$\tau_0 = \sqrt{\tau_e \tau_\sigma}. \quad (2.176)$$

The phase velocity increases with frequency. (The same happens for the Maxwell and Kelvin-Voigt models). The type of dispersion in which this happens is called anomalous dispersion in the electromagnetic terminology. In electromagnetism, the index of refraction – defined as the velocity of light in a vacuum divided by the phase velocity – decreases with frequency for anomalously dispersive media (Born and Wolf, 1964, p. 18; Jones, 1986, p. 644).

The Zener model is suitable to represent relaxation mechanisms such as those illustrated in Figure 2.8b. Processes such as grain-boundary relaxation have to be explained by a distribution of relaxation peaks. This behavior is obtained by considering several

2.4 Mechanical models and wave propagation

Zener elements in series or in parallel, a system which is described in the next section. The phase velocity ranges from $\sqrt{M_R/\rho}$ at the low-frequency limit to $\sqrt{M_U/\rho}$ at the high-frequency limit, and the system exhibits a pure elastic behavior ($Q^{-1} = 0$) at both limits.

2.4.4 Burgers model

A unique model to describe both the transient and steady-state creep process is given by the Burgers model, which is formed with a series connection of a Zener element and a dashpot, or equivalently, a series connection of a Kelvin-Voigt element and a Maxwell element (Klausner, 1991). The model is shown in Figure 2.11, and the constitutive equations of the single elements are

$$\begin{aligned} \sigma_1 &= k_2 \epsilon_2 \\ \sigma_2 &= \eta_2 \partial_t \epsilon_2 = i\omega \eta_2 \epsilon_2 \\ \sigma &= \eta_1 \partial_t \epsilon_3 = i\omega \eta_1 \epsilon_3 \\ \sigma &= k_1 \epsilon_1, \end{aligned} \quad (2.177)$$

where a time Fourier transform is implicit.

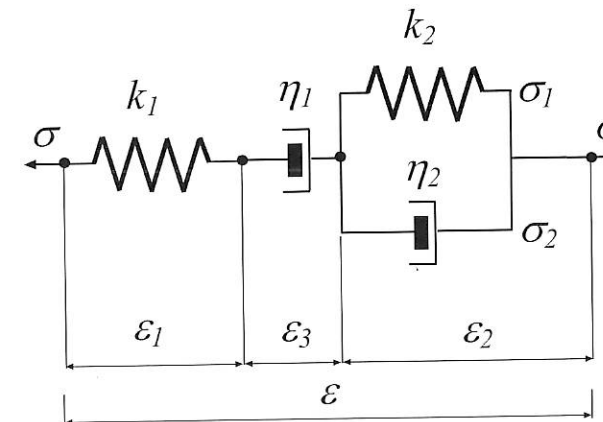


Figure 2.11: Burgers's viscoelastic model. The response of the Burgers model is instantaneous elasticity, delayed elasticity (or viscoelasticity) and viscous flow, the latter described by the series dashpot. On removal of the perturbation, the instantaneous and delayed elasticity are recovered, and it remains the viscous flow. The viscoelastic creep – with steady-state creep – of rocksalt can be described by the Burgers model which includes the transient creep of the Zener model, which does not exhibit steady-state creep, and the steady-state creep of a Maxwell model. (Carcione, Helle and Gangi, 2006).

Since

$$\begin{aligned} \epsilon &= \epsilon_1 + \epsilon_2 + \epsilon_3 \\ \sigma &= \sigma_1 + \sigma_2, \end{aligned} \quad (2.178)$$

we have

$$\sigma = \sigma_1 + \sigma_2 = (k_2 + i\omega \eta_2) \epsilon_2 \quad (2.179)$$

and

$$\epsilon = \epsilon_1 + \epsilon_2 + \epsilon_3 = \frac{\sigma}{k_1} + \frac{\sigma}{i\omega\eta_1} + \frac{\sigma}{k_2 + i\omega\eta_2} \equiv J(\omega)\sigma, \quad (2.180)$$

where

$$J(\omega) = \frac{1}{M(\omega)} = \frac{1}{k_1} + \frac{1}{i\omega\eta_1} + \frac{1}{k_2 + i\omega\eta_2} \quad (2.181)$$

is the complex creep compliance (2.43).

An inverse Fourier transforms of (2.181) and a time integration of the result leads to

$$\partial_t \chi(t) = \frac{\delta(t)}{k_1} + \frac{H(t)}{\eta_1} + \frac{1}{\eta_2} \exp(-t/\tau_\epsilon) H(t) \quad (2.182)$$

and

$$\chi(t) = \left\{ \frac{1}{k_1} + \frac{t}{\eta_1} + \frac{1}{k_2} [1 - \exp(-t/\tau_\epsilon)] \right\} H(t), \quad (2.183)$$

where τ_ϵ is given by equation (2.169)₂. Equation (2.183) can also be obtained by adding the creep functions of the Maxwell (M) and Kelvin-Voigt (KV) models (equations (2.152) and (2.163), respectively), because $\epsilon_2 = \chi_{KV} * \partial_t \sigma$ and $\epsilon_1 + \epsilon_3 = \chi_M * \partial_t \sigma$.

The calculation of the relaxation function is more tricky. The model obeys a time-domain differential equation, which can be obtained by combining equations (2.177) and (2.178):

$$\partial_{tt}^2 \sigma + \left(\frac{k_1}{\eta_1} + \frac{k_1}{\eta_2} + \frac{k_2}{\eta_2} \right) \partial_t \sigma + \frac{k_1 k_2}{\eta_1 \eta_2} \sigma = k_1 \partial_{tt}^2 \epsilon + \frac{k_1 k_2}{\eta_2} \partial_t \epsilon. \quad (2.184)$$

The relaxation function $\psi(t) = \sigma(t)$ is obtained for $\epsilon(t) = H(t)$. Then, factorizing the left-hand side, equation (2.184) can be rewritten as

$$(\omega_1 \delta - \delta') * (\omega_2 \delta - \delta') * \psi = k_1 \delta' + \frac{k_1 k_2}{\eta_2} \delta, \quad (2.185)$$

where $\delta' = \partial_t \delta$, and

$$(2\eta_1 \eta_2) \omega_{1,2} = -b \pm \sqrt{b^2 - 4k_1 k_2 \eta_1 \eta_2}, \quad b = k_1 \eta_1 + k_1 \eta_2 + k_2 \eta_1. \quad (2.186)$$

Hence, the relaxation function is

$$\psi = (\omega_1 \delta - \delta')^{-1} * (\omega_2 \delta - \delta')^{-1} * \left(k_1 \delta' + \frac{k_1 k_2}{\eta_2} \delta \right), \quad (2.187)$$

where here $(\)^{-1}$ denotes the inverse with respect to convolution. Since³

$$(\omega_{1,2} \delta - \delta')^{-1} = -\exp(\omega_{1,2} t) H(t), \quad (2.188)$$

we finally obtain

$$\psi(t) = [A_1 \exp(-t/\tau_1) - A_2 \exp(-t/\tau_2)] H(t), \quad (2.189)$$

where

$$\tau_{1,2} = -\frac{1}{\omega_{1,2}} \quad \text{and} \quad A_{1,2} = \frac{k_1 k_2 + \omega_{1,2} \eta_2 k_1}{\eta_2 (\omega_1 - \omega_2)}. \quad (2.190)$$

³Equation (2.188) is equivalent to $(\omega_{1,2} \delta - \delta') * [-\exp(\omega_{1,2} t) H(t)]$, i.e., $(\omega_{1,2} - \partial_t) [-\exp(\omega_{1,2} t) H(t)] = \delta$, which is identically true.

2.4 Mechanical models and wave propagation

The models studied in the previous sections are limiting cases of the Burgers model. The Maxwell creep function (2.152) is obtained for $k_2 \rightarrow \infty$ and $\eta_2 \rightarrow 0$, where $M_U = k_1$, $\tau = \eta_1/k_1$ and $\tau_\epsilon = 0$. The Kelvin-Voigt creep function (2.163) is obtained for $k_1 \rightarrow \infty$ and $\eta_1 \rightarrow \infty$, where $M_R = k_2$ and $\tau = \tau_\epsilon$. The Zener creep function (2.174) is obtained for $\eta_1 \rightarrow \infty$, where $\tau_1 = \infty$, $\tau_2 = \tau_\sigma$, $A_1 = M_R$ and $A_2 = M_R(\tau_\epsilon/\tau_\sigma - 1)$.

An example of the use of the Burgers model to describe borehole stability is given in Carcione, Helle and Gangi (2006).

2.4.5 Generalized Zener model

As stated before, some processes, as for example, grain-boundary relaxation, have a dissipation factor that is much broader than a single relaxation curve. It seems natural to try to explain this broadening with a distribution of relaxation mechanisms. This approach was introduced by Liu, Anderson and Kanamori (1976) to obtain a nearly constant quality factor over the seismic frequency range of interest. Strictly, their model cannot be represented by mechanical elements, since it requires a spring of negative constant (Casula and Carcione, 1992). Here, we consider the parallel system shown in Figure 2.12, with L Zener elements connected in parallel. The stress-strain relation for each single element is

$$\sigma_l + \tau_{\sigma l} \partial_t \sigma_l = M_{Rl}(\epsilon + \tau_{\epsilon l} \partial_t \epsilon), \quad l = 1, \dots, L, \quad (2.191)$$

where the relaxed moduli are given by

$$M_{Rl} = \frac{k_{1l} k_{2l}}{k_{1l} + k_{2l}}, \quad (2.192)$$

and the relaxation times by

$$\tau_{\sigma l} = \frac{\eta_l}{k_{1l} + k_{2l}}, \quad \tau_{\epsilon l} = \frac{\eta_l}{k_{2l}}. \quad (2.193)$$

According to (2.170), each complex modulus is given by

$$M_l(\omega) = M_{Rl} \left(\frac{1 + i\omega\tau_{\epsilon l}}{1 + i\omega\tau_{\sigma l}} \right). \quad (2.194)$$

The total stress acting on the system is $\sigma = \sum_{l=1}^L \sigma_l$. Therefore, the stress-strain relation in the frequency domain is

$$\sigma = \sum_{l=1}^L M_l \epsilon = \sum_{l=1}^L M_{Rl} \left(\frac{1 + i\omega\tau_{\epsilon l}}{1 + i\omega\tau_{\sigma l}} \right) \epsilon. \quad (2.195)$$

We can choose $M_{Rl} = M_R/L$, and the complex modulus can be expressed as

$$M(\omega) = \sum_{l=1}^L M_l(\omega), \quad M_l(\omega) = \frac{M_R}{L} \left(\frac{1 + i\omega\tau_{\epsilon l}}{1 + i\omega\tau_{\sigma l}} \right), \quad (2.196)$$

thereby reducing the number of independent constants to $2L + 1$.

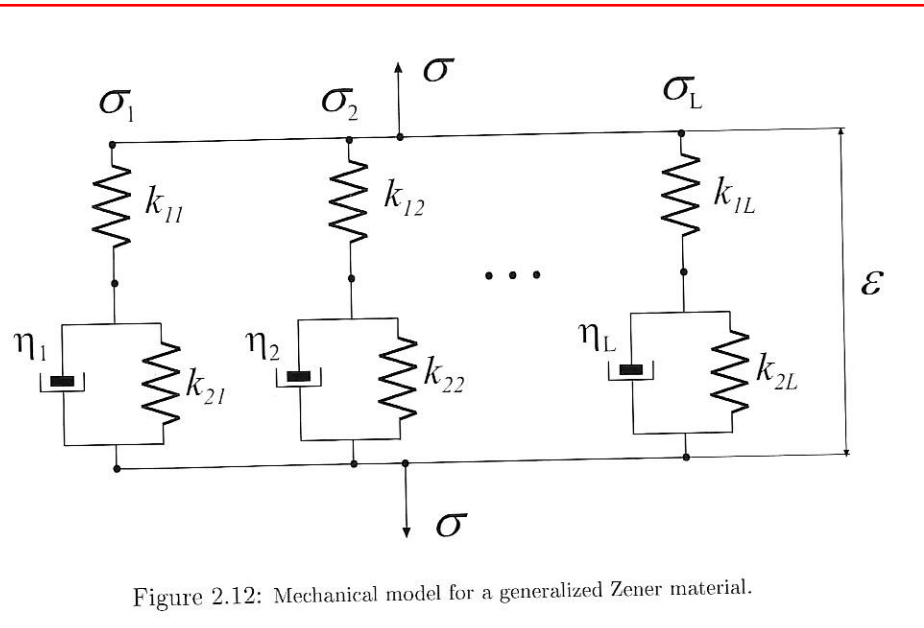


Figure 2.12: Mechanical model for a generalized Zener material.

The relaxation function is easily obtained from the time-domain constitutive equation

$$\sigma = \sum_{l=1}^L \sigma_l = \sum_{l=1}^L \psi_l * \partial_t \epsilon \equiv \psi * \partial_t \epsilon, \quad (2.197)$$

where \$\psi_l\$ has the form (2.173), and

$$\psi(t) = M_R \left[1 - \frac{1}{L} \sum_{l=1}^L \left(1 - \frac{\tau_{el}}{\tau_{\sigma l}} \right) \exp(-t/\tau_{\sigma l}) \right] H(t). \quad (2.198)$$

The unrelaxed modulus is obtained for \$t = 0\$,

$$M_U = M_R \left[1 - \frac{1}{L} \sum_{l=1}^L \left(1 - \frac{\tau_{el}}{\tau_{\sigma l}} \right) \right] = \frac{M_R}{L} \sum_{l=1}^L \frac{\tau_{el}}{\tau_{\sigma l}}. \quad (2.199)$$

The relaxation function obtained by Liu, Anderson and Kanamori (1976) lacks the factor \$1/L\$.

Nearly constant \$Q\$

In oil prospecting and seismology, constant-\$Q\$ models are convenient to parameterize attenuation in rocks, since the frequency dependence is usually not known. Moreover, there is physical evidence that attenuation is almost linear with frequency – therefore \$Q\$ is constant – in many frequency bands (McDonald, Angona, Milss, Sengbush, van Nostrand and White, 1958). The technique to obtain a nearly constant \$Q\$ over a given frequency range is to consider equispaced relaxation mechanisms in a \$\log(\omega)\$ scale (Liu, Anderson

2.4 Mechanical models and wave propagation

and Kanamori, 1976). We show, in the following discussion, how to obtain a constant-\$Q\$ model for low-loss solids by using a simple algorithm, without curve fitting of the \$Q\$ factor.

A more physical parameterization of a single Zener element can be obtained with the center frequency \$\omega_0 = \tau_0^{-1}\$, and the value of the quality factor at this frequency,

$$Q_0 = \frac{2\tau_0}{\tau_\epsilon - \tau_\sigma}. \quad (2.200)$$

The quality factor (2.175) becomes

$$Q(\omega) = Q_0 \left(\frac{1 + \omega^2 \tau_0^2}{2\omega \tau_0} \right). \quad (2.201)$$

Solving for \$\tau_\sigma\$ and \$\tau_\epsilon\$ in equations (2.176) and (2.200), we obtain

$$\tau_\epsilon = \frac{\tau_0}{Q_0} \left(\sqrt{Q_0^2 + 1} + 1 \right) \quad \text{and} \quad \tau_\sigma = \frac{\tau_0}{Q_0} \left(\sqrt{Q_0^2 + 1} - 1 \right). \quad (2.202)$$

Now, the problem is to find a set of relaxation times \$\tau_{el}\$ and \$\tau_{\sigma l}\$ that gives an almost constant quality factor \$Q\$ in a given frequency band centered at \$\omega_{0m} = 1/\tau_{0m}\$. This is the location of the mechanism situated at the middle of the band, which, for odd \$L\$, has the index \$m = L/2 - 1\$. As mentioned above, single relaxation peaks should be taken equidistant in a \$\log(\omega)\$ scale. The quality factor of the system is

$$Q(\omega) = \frac{\text{Re}(M)}{\text{Im}(M)} = \frac{\text{Re}(\sum_{l=1}^L M_l)}{\text{Im}(\sum_{l=1}^L M_l)}, \quad (2.203)$$

where \$M_l\$ is given in equation (2.196)₂. Since \$Q_l = \text{Re}(M_l)/\text{Im}(M_l)\$ is the quality factor of each element, equation (2.203) becomes

$$Q(\omega) = \frac{\sum_{l=1}^L Q_l \text{Im}(M_l)}{\sum_{l=1}^L \text{Im}(M_l)}, \quad (2.204)$$

where

$$Q_l(\omega) = Q_{0l} \left(\frac{1 + \omega^2 \tau_{0l}^2}{2\omega \tau_{0l}} \right). \quad (2.205)$$

Using equation (2.200) and assuming the low-loss approximation (\$\tau_{\sigma l} \approx \tau_{0l}\$), we have

$$\text{Im}(M_l) = \frac{M_R}{L} \left[\frac{\omega(\tau_{el} - \tau_{\sigma l})}{1 + \omega^2 \tau_{\sigma l}^2} \right] \approx \frac{M_R}{L} \left[\frac{2\omega \tau_{0l}}{Q_{0l}(1 + \omega^2 \tau_{0l}^2)} \right] = \frac{M_R}{L Q_l}. \quad (2.206)$$

We now choose \$Q_{0l} = Q_0\$, and substitute equation (2.206) into equation (2.204) to obtain

$$Q(\omega) = L Q_0 \left(\sum_{l=1}^L \frac{2\omega \tau_{0l}}{1 + \omega^2 \tau_{0l}^2} \right)^{-1}. \quad (2.207)$$

We choose \$\tau_{0l}\$ regularly distributed in the \$\log(\omega)\$ axis, and \$Q(\omega_{0m}) = \bar{Q}\$, the desired value of the quality factor.

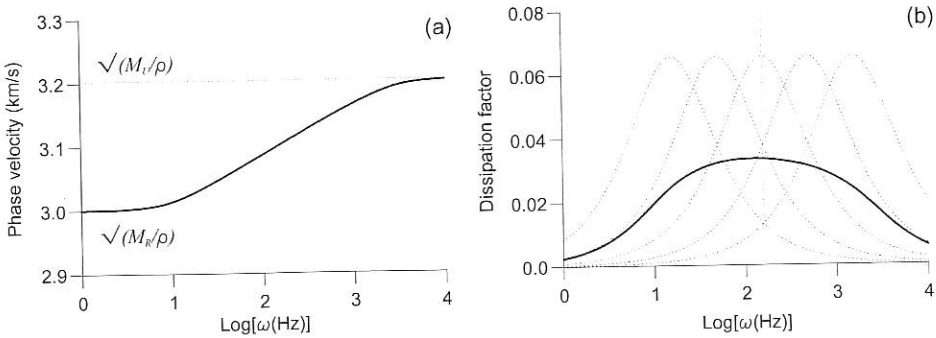


Figure 2.13: Phase velocity (a) and dissipation factor (b) of the generalized Zener model.

Thus, the choice

$$Q_0 = \bar{Q} \sum_{l=1}^L \frac{2\omega_{0m}\tau_{0l}}{1 + \omega_{0m}^2\tau_{0l}^2} \quad (2.208)$$

gives a constant Q (equal to \bar{Q}), as can be verified by substitution of (2.208) into (2.207).

Figure 2.13 shows the phase velocity (a) and the dissipation factor (b) versus frequency, for five dissipation mechanisms – each with a quality-factor parameter $Q_0 = 15$, such that $\bar{Q} = 30$. The dotted curves are the quality factor of each single mechanism, and the vertical dotted line indicates the location of the third relaxation peak. The relaxation function of the nearly constant- Q model is shown in Figure 2.14.

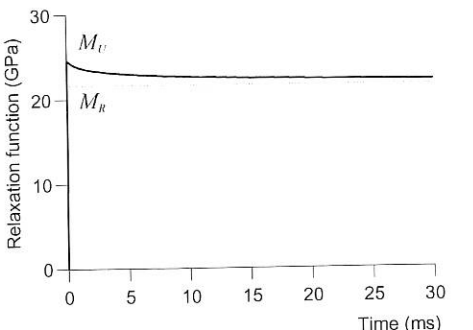


Figure 2.14: Relaxation function of the generalized Zener model.

2.4.6 Nearly constant- Q model with a continuous spectrum

A linear and continuous superposition of Zener elements, where each element has equal weight, gives a continuous relaxation spectrum with a constant quality factor over a given frequency band (Liu, Anderson and Kanamori, 1976; Ben-Menahem and Singh, 1981, p.

2.5 Constant- Q model and wave equation

911). The resulting relaxation function exhibits elastic (lossless) behavior in the low- and high-frequency limits. Its frequency-domain form is

$$M(\omega) = M_R \left[1 + \frac{2}{\pi \bar{Q}} \ln \left(\frac{1 + i\omega\tau_2}{1 + i\omega\tau_1} \right) \right]^{-1}, \quad (2.209)$$

where τ_1 and τ_2 are time constants, with $\tau_2 < \tau_1$, and \bar{Q} defines the value of the quality factor, which remains nearly constant over the selected frequency band. The low-frequency limit of M is M_R , and we can identify this modulus with the elastic modulus. Alternatively, we may consider

$$M(\omega) = M_U \left[1 + \frac{2}{\pi \bar{Q}} \ln \left(\frac{\tau_2^{-1} + i\omega}{\tau_1^{-1} + i\omega} \right) \right]^{-1}, \quad (2.210)$$

whose high-frequency limit is the elastic modulus M_U . These functions give a nearly constant quality factor in the low-loss approximation. Figure 2.15 represents the dissipation factor $Q^{-1} = \text{Im}(M)/\text{Re}(M)$ for the two functions (2.209) and (2.210) (solid and dashed lines, respectively).

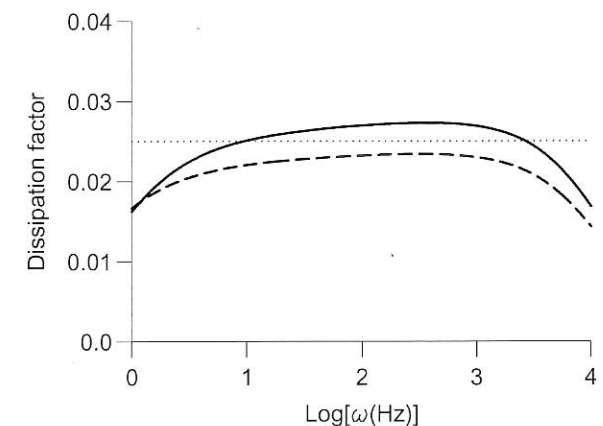


Figure 2.15: Dissipation factors for the nearly constant- Q model, corresponding to the two functions (2.209) and (2.210) (solid and dashed lines, respectively). The curves correspond to $\bar{Q} = 40$, $\tau_1 = 1.5$ s and $\tau_2 = 8 \times 10^{-5}$ s. The dotted line represents \bar{Q}^{-1} .

2.5 Constant- Q model and wave equation

A perfect constant- Q model can be designed for all frequencies. Bland (1960), Caputo and Mainardi (1971), Kjartansson (1979), Müller (1983) and Mainardi and Tomirotti (1998) discuss a linear attenuation model with the required characteristics, but the idea is much older (Nutting, 1921; Scott Blair, 1949). The so-called Kjartansson's constant- Q model – in seismic prospecting literature – is based on a creep function of the form $t^{2\gamma}$,

where t is time and $\gamma \ll 1$ for seismic applications. This model is completely specified by two parameters, i.e., phase velocity at a reference frequency and Q . Therefore, it is mathematically much simpler than any nearly constant Q , such as, for instance, a spectrum of Zener models (Carcione, Kosloff and Kosloff, 1988b,c,d). Due to its simplicity, Kjartansson's model is used in many seismic applications, mainly in its frequency-domain form.

The relaxation function is

$$\psi(t) = \frac{M_0}{\Gamma(1-2\gamma)} \left(\frac{t}{t_0}\right)^{-2\gamma} H(t), \quad (2.211)$$

where M_0 is a bulk modulus, Γ is Euler's Gamma function, t_0 is a reference time and γ is a dimensionless parameter. The parameters M_0 , t_0 and γ have precise physical meanings that will become clear in the following analysis.

Using equation (2.31) and after some calculations, we get the complex modulus,

$$M(\omega) = M_0 \left(\frac{i\omega}{\omega_0}\right)^{2\gamma}, \quad (2.212)$$

where $\omega_0 = 1/t_0$ is the reference frequency.

2.5.1 Phase velocity and attenuation factor

The complex velocity is given by equation (2.80),

$$v_c = \sqrt{\frac{M}{\rho}}, \quad (2.213)$$

and the phase velocity can be obtained from equation (2.83),

$$v_p = c_0 \left| \frac{\omega}{\omega_0} \right|^{\gamma} \quad (2.214)$$

with

$$c_0 = \sqrt{\frac{M_0}{\rho}} \left[\cos\left(\frac{\pi\gamma}{2}\right) \right]^{-1}. \quad (2.215)$$

The attenuation factor (2.85) is given by

$$\alpha = \tan\left(\frac{\pi\gamma}{2}\right) \operatorname{sgn}(\omega) \frac{\omega}{v_p}, \quad (2.216)$$

and the quality factor, according to equation (2.120), is

$$Q = \frac{1}{\tan(\pi\gamma)}. \quad (2.217)$$

Firstly, we have from equation (2.214) that c_0 is the phase velocity at $\omega = \omega_0$ (the reference frequency), and that

$$M_0 = \rho c_0^2 \cos^2\left(\frac{\pi\gamma}{2}\right). \quad (2.218)$$

2.5 Constant- Q model and wave equation

Secondly, it follows from equation (2.217) that Q is independent of frequency, so that

$$\gamma = \frac{1}{\pi} \tan^{-1}\left(\frac{1}{Q}\right) \quad (2.219)$$

parameterizes the attenuation level. Hence, we see that $Q > 0$ is equivalent to $0 < \gamma < 1/2$. Moreover, $v_p \rightarrow 0$ when $\omega \rightarrow 0$, and $v_p \rightarrow \infty$ when $\omega \rightarrow \infty$. It follows that very high frequencies of the signal propagate at almost infinite velocity, and the differential equation describing the wave motion is parabolic (e.g., Prüss, 1993).

2.5.2 Wave equation in differential form. Fractional derivatives.

Let us consider propagation in the (x, z) -plane and a 2-D wave equation of the form

$$\frac{\partial^\beta w}{\partial t^\beta} = b\Delta w + f_w, \quad (2.220)$$

where $w(x, z, t)$ is a field variable, β is the order of the time derivative, b is a positive parameter, Δ is the 2-D Laplacian operator

$$\Delta = \partial_1^2 + \partial_3^2, \quad (2.221)$$

and f_w is a forcing term. Consider a plane wave

$$\exp[i(\omega t - k_1 x - k_3 z)], \quad (2.222)$$

where ω is real and (k_1, k_3) is the complex wavevector. Substitution of the plane wave (2.222) in the wave equation (2.220) with $f_w = 0$ yields the dispersion relation

$$(i\omega)^\beta + bk^2 = 0, \quad (2.223)$$

where $k = \sqrt{k_1^2 + k_3^2}$ is the complex wavenumber. Equation (2.223) is the Fourier transform of equation (2.220). The properties of the Fourier transform when it acts on fractional derivatives are well established, and a rigorous treatment is available in the literature (e.g., Dattoli, Torre and Mazzacurati, 1998). Since $k^2 = \rho\omega^2/M$, a comparison of equations (2.223) and (2.212) gives

$$\beta = 2 - 2\gamma, \quad \text{and} \quad b = \left(\frac{M_0}{\rho}\right) \omega_0^{-2\gamma}. \quad (2.224)$$

Equation (2.220), together with (2.224), is the wave equation corresponding to Kjartansson's stress-strain relation (Kjartansson, 1979). In order to obtain realistic values of the quality factor, which correspond to wave propagation in rocks, $\gamma \ll 1$ and the time derivative in equation (2.220) has a fractional order.

Kjartansson's wave equation (2.220) is a particular version of a more general wave equation for variable material properties. The convolutional stress-strain relation (2.28) can be written in terms of fractional derivatives. In fact, it is easy to show, using equations (2.212) and (2.224), that it is equivalent to

$$\sigma = \rho b \frac{\partial^{2-\beta} \epsilon}{\partial t^{2-\beta}}. \quad (2.225)$$

HANDBOOK OF GEOPHYSICAL EXPLORATION

SECTION I. SEISMIC EXPLORATION

Editors: Klaus Helbig and Sven Treitel

Volume

1. Basic Theory in Reflection Seismology
2. Seismic Instrumentation, 2nd Edition
3. Seismic Field Techniques
- 4A. Seismic Inversion and Deconvolution: Classical Methods
- 4B. Seismic Inversion and Deconvolution: Dual-Sensor Technology
5. Seismic Migration (Theory and Practice)
6. Seismic Velocity Analysis
7. Seismic Noise Attenuation
8. Structural Interpretation
9. Seismic Stratigraphy
10. Production Seismology
11. 3-D Seismic Exploration
12. Seismic Resolution
13. Refraction Seismics
14. Vertical Seismic Profiling: Principles
3rd Updated and Revised Edition
- 15A. Seismic Shear Waves: Theory
- 15B. Seismic Shear Waves: Applications
- 16A. Seismic Coal Exploration: Surface Methods
- 16B. Seismic Coal Exploration: In-Seam Seismics
17. Mathematical Aspects of Seismology
18. Physical Properties of Rocks
19. Shallow High-Resolution Reflection Seismics
20. Pattern Recognition and Image Processing
21. Supercomputers in Seismic Exploration
22. Foundations of Anisotropy for Exploration Seismics
23. Seismic Tomography
24. Borehole Acoustics
25. High Frequency Crosswell Seismic Profiling
26. Applications of Anisotropy in Vertical Seismic Profiling
27. Seismic Multiple Elimination Techniques
28. Wavelet Transforms and Their Applications to Seismic Data
Acquisition, Compression, Processing and Interpretation
29. Seismic Signatures and Analysis of Reflection Data in Anisotropic Media
30. Computational Neural Networks for Geophysical Data Processing
31. Wave Fields in Real Media: Wave Propagation in Anisotropic,
Anelastic and Porous Media
32. Nuclear Magnetic Resonance Petrophysical and Logging Applications
33. Seismic Amplitude Inversion in Reflection Tomography
34. Seismic Waves and Rays in Elastic Wave Media
35. Seismic While Drilling: Fundamentals of Drill-Bit Seismic for Exploration
36. Information-based Inversion and Processing with Applications
37. Seismic Stratigraphy, Basin Analysis and Reservoir Characterisation
38. Wave Fields in Real Media: Wave Propagation in Anisotropic, Anelastic
Porous and Electromagnetic Media
(Second Edition, Revised and Extended)

SECTION I. SEISMIC EXPLORATION

Volume 38

WAVE FIELDS IN REAL MEDIA:

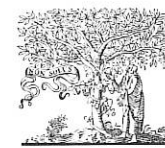
Wave Propagation in Anisotropic, Anelastic, Porous
and Electromagnetic Media

(SECOND EDITION, REVISED AND EXTENDED)

by

José M. CARCIONE

Istituto Nazionale di Oceanografia e di Geofisica Sperimentale (OGS),
Borgo Grotta Gigante 42c, 34010 Sgonico, Trieste, Italy



ELSEVIER

Amsterdam – Boston – Heidelberg – London – New York – Oxford
Paris – San Diego – San Francisco – Singapore – Sydney – Tokyo